Turk J Elec Eng & Comp Sci, Vol.20, No.4, 2012, © TÜBİTAK
doi:10.3906/elk-1011-915

Research on cutoff wavelength of dominant mode and field patterns in trapezoidal microshield lines

Hai SUN[1,2,*], **Yujiang WU**[2]
[1] *School of Mathematics and Informational Sciences, East China Institute of Technology, Fuzhou, 344000, P.R. CHINA*
e-mail: sunhai0804@126.com
[2] *School of Mathematics and Statistics, Lanzhou University, Lanzhou, 730000, P.R. CHINA*

Received: 04.11.2010

Abstract

The influence of the position of the metallic signal strip on the cutoff characteristic of the dominant mode and the field patterns in 3 types of trapezoidal microshield lines are calculated by the edge-based finite element method. These trapezoidal microshield lines include trapezoidal microshield lines with a single signal line, dual signal lines, and 3 signal lines. The cutoff wavelength of the dominant mode can be adjusted by changing the dimensions of metallic signal strips as well as by adjusting their positions. Field patterns of the dominant mode and the first-higher-order mode for different dimensions and the dielectric constant of the dielectric substrate are also illustrated. The numerical results in this article provide an extension of the existing design data of trapezoidal microshield lines and are useful in practical applications.

Key Words: *Cutoff wavelength of dominant mode, field patterns, single signal line, dual signal lines, three signal lines, trapezoidal microshield line, edge-based finite element method*

1. Introduction

Recently, microshield lines have received considerable attention in microwave integrated circuit and monolithic microwave integrated circuit designs. Microshield lines may be considered as part of the evolution of the conventional microstrip or coplanar structure; however, they present a solution to the technology problems encountered in the design of conventional microstrips. Compared to conventional transmission lines, microshield lines can operate without the need for via holes or the use of air bridges for ground equalization, and they supply a wide range of impedance. In addition, they can reduce radiation loss and reduce electromagnetic coupling between adjacent lines [1]. Various types of microshield lines have been discussed in the last decade. Yuan and Lin analyzed the characteristic impedance in V-shaped, circular, and elliptical microshield lines [2]. Cheng and Robertson and Yan and Pramanick studied the characteristic impedance in asymmetrical V-shaped microshield

*Corresponding author: School of Mathematics and Informational Sciences, East China Institute of Technology, Fuzhou, 344000, P.R. CHINA

lines and W-shaped microshield lines [3,4]. Kiang calculated the characteristic impedance of microshield lines with an arbitrary shield cross-section [5]. Full wave analysis can provide more accuracy than any of the other methods in calculating transmission characteristics of inhomogeneous waveguide structure, so the finite element method and the edge-based finite element method have enjoyed popularity; for example, Lu and Leonard and Sun and Lu analyzed several different kinds of waveguide structures and microshield lines by the finite element method and the edge-based finite element method [6-10].

Based on the edge-based finite element method, this article will discuss the cutoff wavelength of the dominant mode and the field patterns in trapezoidal microshield lines with a single signal line (TML-S), trapezoidal microshield lines with dual signal lines (TML-D), and trapezoidal microshield lines with 3 signal lines (TML-T). The cutoff wavelength and the field patterns for different dimensions and positions of the metallic signal strips are presented. It should be mentioned that we solved 2D problems.

2. Theoretical analysis

Figure 1 shows the cross-section of the trapezoidal lines, where parameters a, h_1, h_2, c, and c_5 are used to define the outer dimensions of the microshield line; b, b_1, b_2, and b_3 and t, t_1, t_2, and t_3 are the width and thickness of the metallic signal strips, respectively; c_1, c_2, c_3, and c_4 are used to measure the position of the metallic signal strips; and the relative permittivity is ε_r. We assumed that $h_1/a = 0.3$ and $h_2/a = 0.2$. Because of the dielectric substrate, the electromagnetic waves are a combination of the transverse magnetic (TM) mode and transverse electric (TE) mode. Both E_z and H_z exist simultaneously. In the trapezoidal microshield lines, modes may generally be described as quasi-longitudinal section magnetic or quasi-longitudinal section electric, depending on whether E_x and E_y are equal to zero.

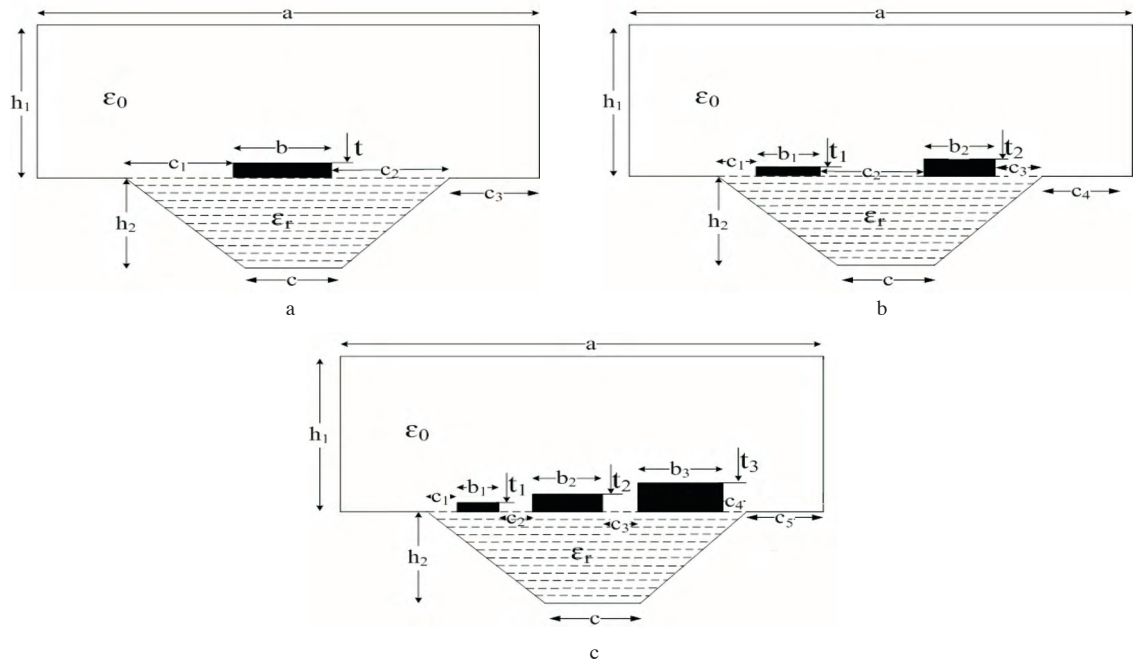

Figure 1. Cross-sections of the trapezoidal microshield lines: a) single signal line; b) dual signal lines; c) 3 signal lines.

Maxwell's equations can be written as:

$$\begin{cases} \nabla_t \times \overrightarrow{H} = j\omega\varepsilon_r\varepsilon_0 \overrightarrow{E} \\ \nabla_t \times \overrightarrow{E} = -j\omega\mu_r\mu_0 \overrightarrow{H} \end{cases} . \tag{1}$$

The boundary conditions can be written as:

$$\hat{n} \times \overrightarrow{E} = 0 \quad \text{on electric walls,} \tag{2}$$

$$\hat{n} \times \left(\nabla_t \times \overrightarrow{E}\right) = 0 \quad \text{on magnetic walls.} \tag{3}$$

The outer domain was modeled as a magnetic wall where ε_0 and μ_0 represent the permittivity and permeability of free space, respectively. ε_r and μ_r represent the relative permittivity and permeability, respectively. From Eq. (1), we can obtain the vector Helmholtz equation:

$$\nabla_t \times \left(\frac{1}{\varepsilon_r}\nabla_t \times \overrightarrow{H}\right) - k_c^2\mu_r\overrightarrow{H} = 0. \tag{4}$$

Here k_c^2 expresses the cutoff wave number and ∇_t expresses the transversal nabla operator Eq. (2) can be solved by using either the node-based finite element method or the edge-based finite element method. Unfortunately, the node-based finite element method when applied to the inhomogeneous waveguide problem will result in spurious solutions, which are generally attributed to the lack of enforcement of the divergence condition [11]. On the contrary, the edge-based finite element method completely eliminates the spurious modes by assigning degrees of freedom to the edges [12].

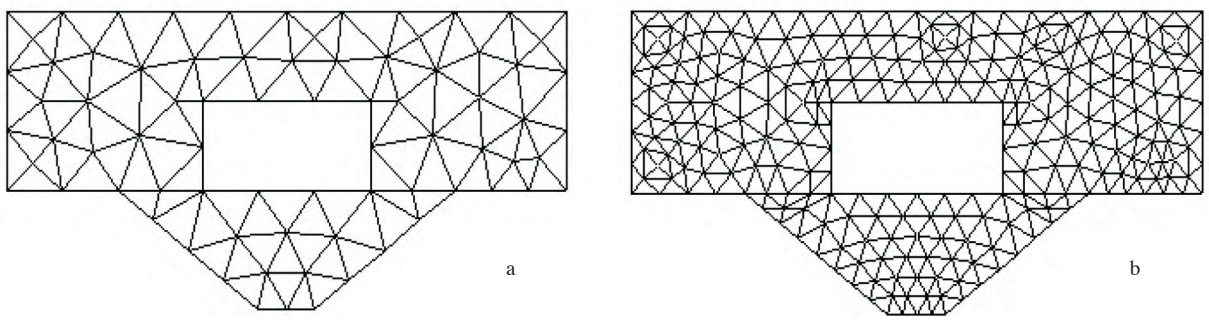

Figure 2. An example of triangulation subdivision of TML-S: a) initial mesh; b) refined mesh.

For this reason, the edge-based finite element method was employed in this study. The cross-sections of the trapezoidal lines were divided into a number of triangular elements. Taken as an example, Figure 2 shows the schematic diagrams of the triangulation subdivision of TML-S; in the initial mesh, there are 77 nodes and 113 triangular elements, and in the refined mesh, there are 267 nodes and 452 triangular elements. The accuracy can be improved by increasing the element number. Using the edge-based finite element method procedures for Eq. (4) leads to the following eigenvalue matrix:

$$\begin{bmatrix} S(tt) & S(tz) \\ S(zt) & S(zz) \end{bmatrix} \begin{bmatrix} h_t \\ h_z \end{bmatrix} = k_c^2 \begin{bmatrix} T(tt) & 0 \\ 0 & T(zz) \end{bmatrix} \begin{bmatrix} h_t \\ h_z \end{bmatrix}, \tag{5}$$

where $S(tt)$, $S(tz)$, $S(zt)$, $S(zz)$, $T(tt)$, and $T(zz)$ are known matrices; h_t is approximated by edge elements whereas h_z is approximated by nodal elements; and t and z represent the transverse direction and the z direction, respectively [11]. Eq. (5) can be written in the following matrix form:

$$[S][\phi] = k_c^2 [T][\phi]. \tag{6}$$

Here, k_c^2 represents the cutoff wavenumber and the smallest k_c^2 is the eigenvalue of the dominant mode. The cutoff wavelength of the dominant mode and the field patterns can be calculated by solving Eq. (6) as a generalized eigenvalue problem.

3. Results and discussion

To verify the accuracy of the edge-based finite element method presented here, the Table gives comparisons between the computed results in this paper for the cutoff wavelength of the dielectric-loaded double-ridged waveguide and the literature data. The results in this paper agree well with those of [9,13], and so the method in this paper is proven to be accurate enough.

Table. Comparisons of the cutoff wavenumbers in the dielectric-loaded double-ridged waveguide ($\varepsilon_r = 1.5\varepsilon_0, a = 12.7, b = 10.16, s = 2.54, d = 2.79$).

	Cutoff wavenumber				
TE modes	This article	[9]	Error (%)	[13]	Error (%)
Dominant	0.1313	0.1307	0.5	0.1291	1.7
First higher	0.3162	0.3153	0.3	0.3137	0.5
Second higher	0.5207	0.5196	0.2	0.5080	2.5
Third higher	0.6249	0.6238	0.2	0.6190	1.0
Fourth higher	0.6571	0.6518	0.9	0.6550	0.3
Fifth higher	0.7051	0.7059	0.1	0.6931	1.7

Next we calculate the cutoff wavelength of the dominant mode and the field patterns in TML-S, TML-D, and TML-T. It is a vast task to find the solution of the cutoff wavelength with different ε_r values, so we assume the dielectric constant $\varepsilon_r = 2.55$. When we illustrate the field patterns of the dominant mode and the first-higher-order mode in 3 types of trapezoidal microshield lines, however, we assume the dielectric constant $\varepsilon_r = 2.55$, 5, and 10.

3.1. The cutoff wavelength of the dominant mode and the field patterns in TML-S

Figures 3 and 4 show the variations of the normalized cutoff wavelength of the dominant mode in TML-S for different values of t/h_1, b/a, and c/a. Figures 5 and 6 show the field patterns of the dominant mode and the first-higher-order mode in TML-S for different ε_r values. From these Figures, we can conclude the following points.

1. For fixed c/a, c_1/a, c_2/a, c_3/a, and b/a, the values of normalized cutoff wavelengths of the dominant mode increase as t/h_1 increases from 0.1 to 0.9.

2. For fixed c/a, c_1/a, c_3/a, b/a, and t/h_1, the cutoff wavelengths increase as c_2/a changes from 0.1 to 0.4.

3. For fixed c/a, c_1/a, c_2/a, andb/a, when t/h_1 changes from 0.1 to 0.5, the cutoff wavelengths decrease as c_3/a changes from 0.1 to 0.4, but when t/h_1 changes from 0.5 to 0.9, the cutoff wavelengths increase as c_3/a changes from 0.1 to 0.4.

4. For fixed c/a, c_1/a, c_2/a, c_3/a, andt/h_1, the cutoff wavelengths increase as b/a increases from 0.1 to 0.8. One point that needs to be emphasized is that when b/aincreases from 0.6 to 0.8, the cutoff wavelengths increase very fast; the reason for this may be that the region of the dielectric substrate increases rapidly.

5. For fixed c_1/a, c_2/a, c_3/a, b/a, and t/h_1, the cutoff wavelengths also increase as c/a changes from 0.1 to 0.8.

6. For smaller values of the dielectric constant, such as $\varepsilon_r = 2.22$ or 5.0, the electric field lines of the dominant mode are averagely distributed in the cross-section, while the electric field lines of the first-higher-order mode are mainly concentrated in the dielectric substrate.

7. As the values of the dielectric constant increase, such as$\varepsilon_r = 10$, the field patterns are completely reversed. The electric field lines of the dominant mode are distributed with a concentration in the dielectric substrate, while the electric field lines of the first-higher-order mode are distributed evenly in the cross-section.

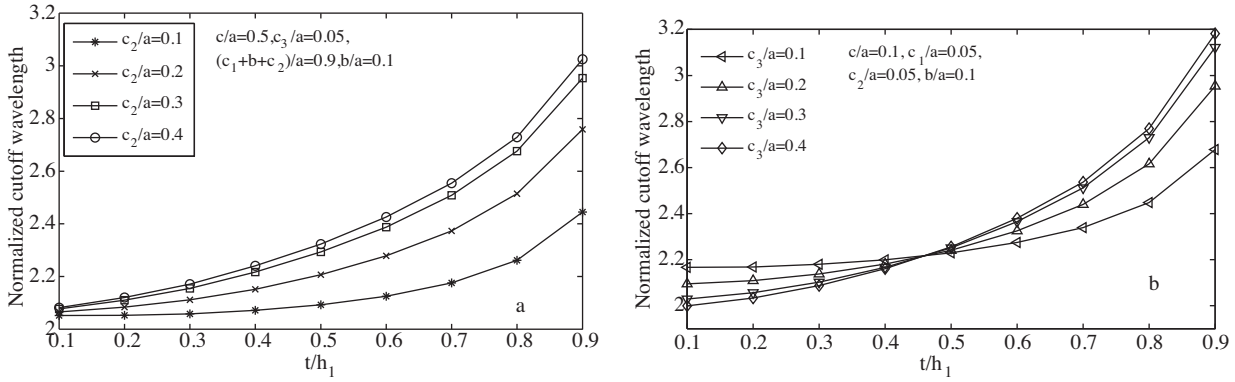

Figure 3. Normalized cutoff wavelength of dominant mode in TML-S versus t/h_1: a) varied c_2/a; b) varied c_3/a.

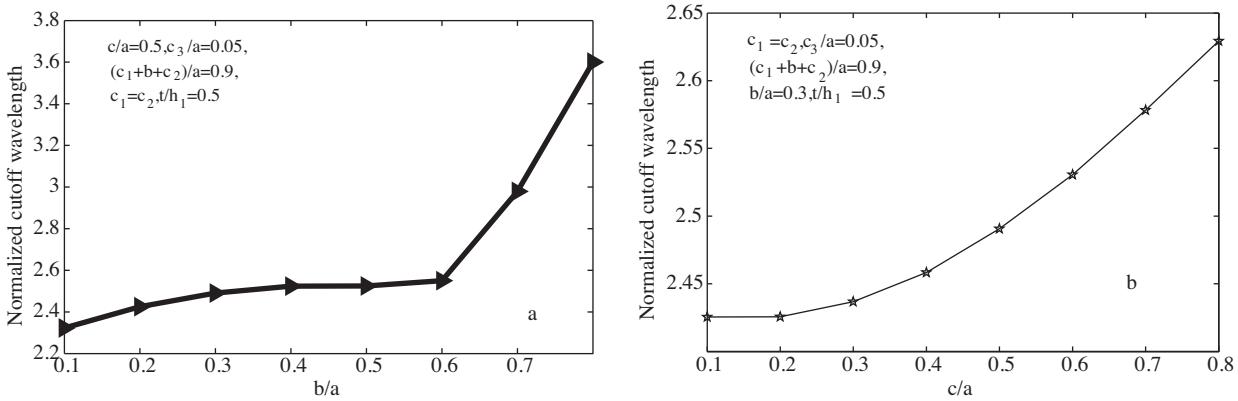

Figure 4. Normalized cutoff wavelength of dominant mode in TML-S: a) versusb/a; b) versus c/a.

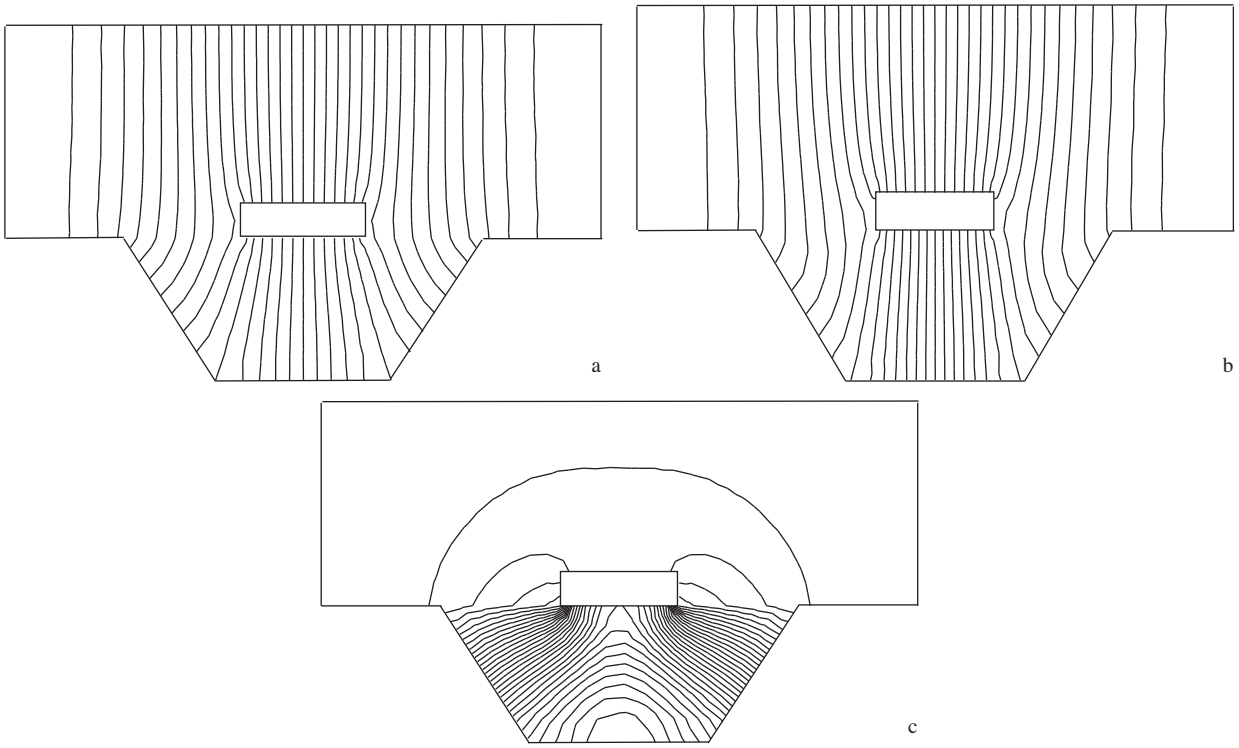

Figure 5. Field patterns of the dominant mode in TML-S ($c/a = 0.3, c_1/a = c_2/a = 0.15, c_3/a = 0.25, t/a = 0.05, b/a = 0.2$): a) $\varepsilon_r = 2.55$; b) $\varepsilon_r = 5$; c) $\varepsilon_r = 10$.

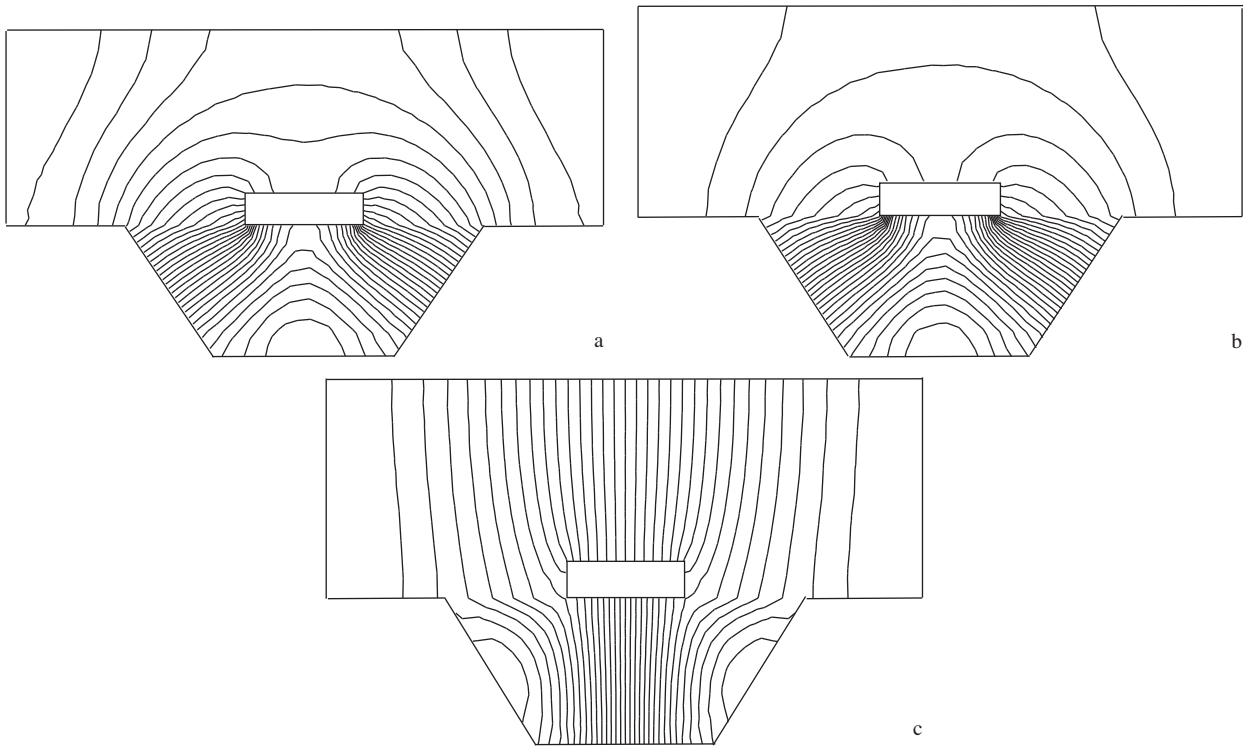

Figure 6. Field patterns of the first-higher-order mode in TML-S ($c/a = 0.3, c_1/a = c_2/a = 0.15, c_3/a = 0.25, t/a = 0.05, b/a = 0.2$): a) $\varepsilon_r = 2.55$; b) $\varepsilon_r = 5$; c) $\varepsilon_r = 10$.

3.2. The cutoff wavelength of the dominant mode and the field patterns in TML-D

The variations of the normalized cutoff wavelength of the dominant mode in TML-D for different values of t_1/h_1, t_2/h_1, b_1/a, b_2/a, c_1/a, c_2/a, and c_4/a are shown in Figures 7 and 8. Figures 9-12 show the field patterns of the dominant mode and the first-higher-order mode in TML-D for different ε_r values. From these Figures, we can conclude:

1. For fixed c/a, c_1/a, c_2/a, c_3/a, c_4/a, b_1/a, and b_2/a, the values of normalized cutoff wavelengths of the dominant mode increase as t_2/h_1 and $t_1/h_1 = t_2/h_1$ increase from 0.1 to 0.9.

2. For fixed c/a, c_1/a, c_3/a, c_4/a, b_2/a, t_1/h_1, andt_2/h_1, the cutoff wavelengths also increase as b_1/a increases from 0.1 to 0.65.

3. For fixed c/a, c_1/a, c_3/a, c_4/a, t_1/h_1, andt_2/h_1, the cutoff wavelengths first decrease and then increase as $b_1/a = b_2/a$ increases from 0.05 to 0.35.

4. For fixed c/a, c_3/a, c_4/a, b_1/a, b_2/a, t_1/h_1, and t_2/h_1, the cutoff wavelengths first increase and then decrease as c_1/a increases from 0.1 to 0.6.

5. For fixed c/a, c_1/a, c_4/a, b_1/a, b_2/a, t_1/h_1, andt_2/h_1, the cutoff wavelengths also first increase and then decrease as c_2/a increases from 0.1 to 0.6.

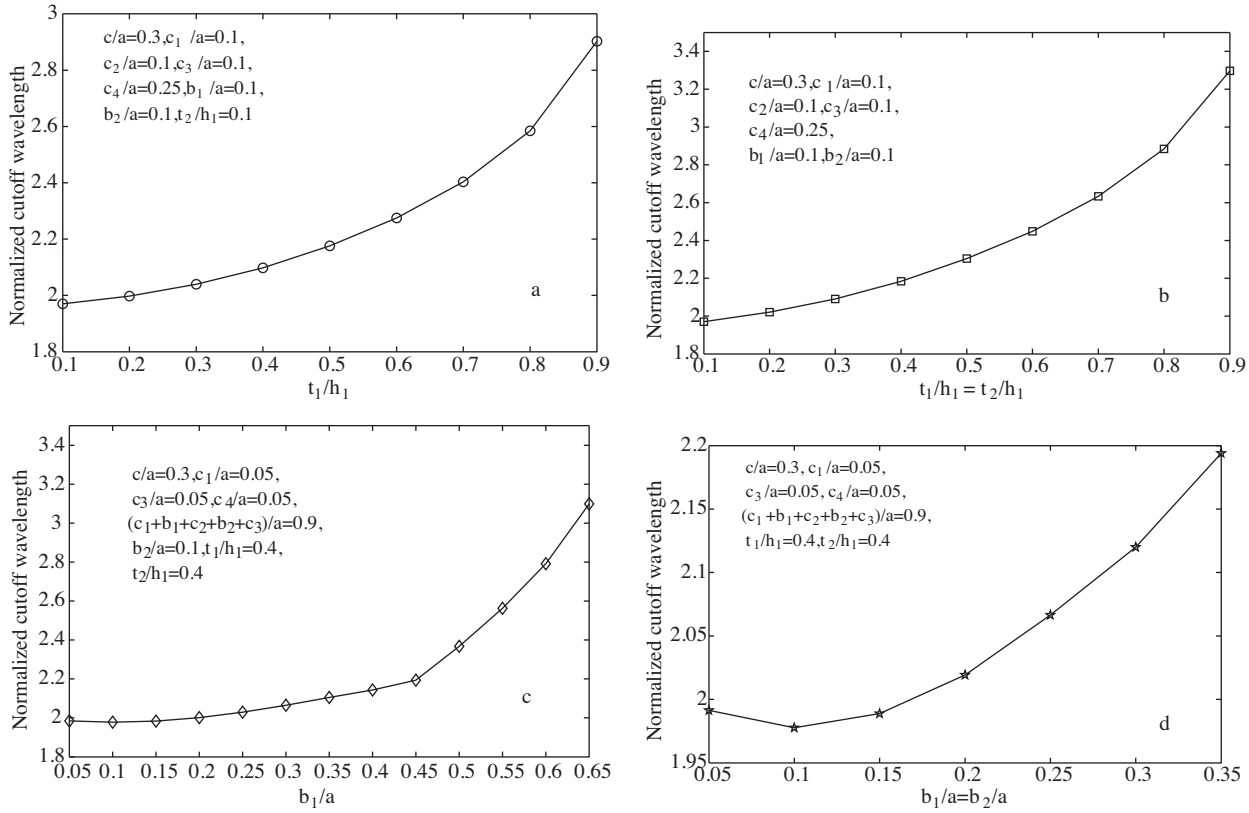

Figure 7. Normalized cutoff wavelength of dominant mode in TML-D: a) versust_1/h_1; b) versus $t_1/h_1 = t_2/h_1$; c) versus b_1/a; d) versus $b_1/a = b_2/a$.

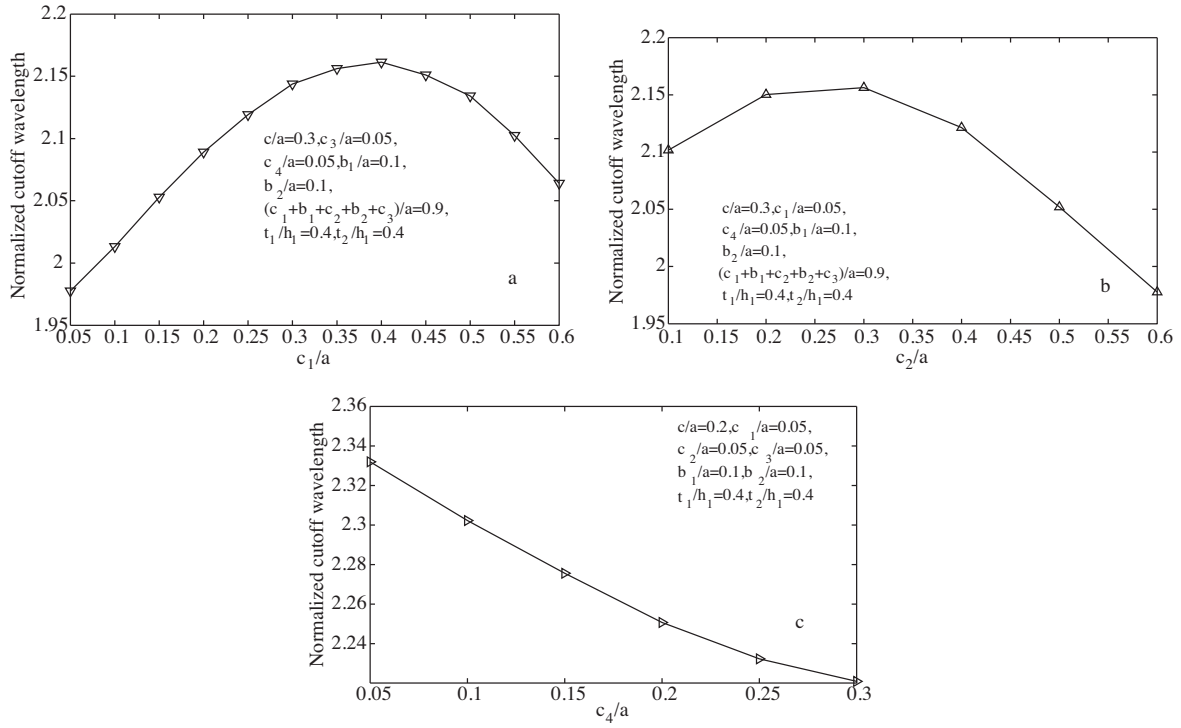

Figure 8. Normalized cutoff wavelength of dominant mode in TML-D: a) versus c_1/a; b) versus c_2/a; c) versus c_4/a.

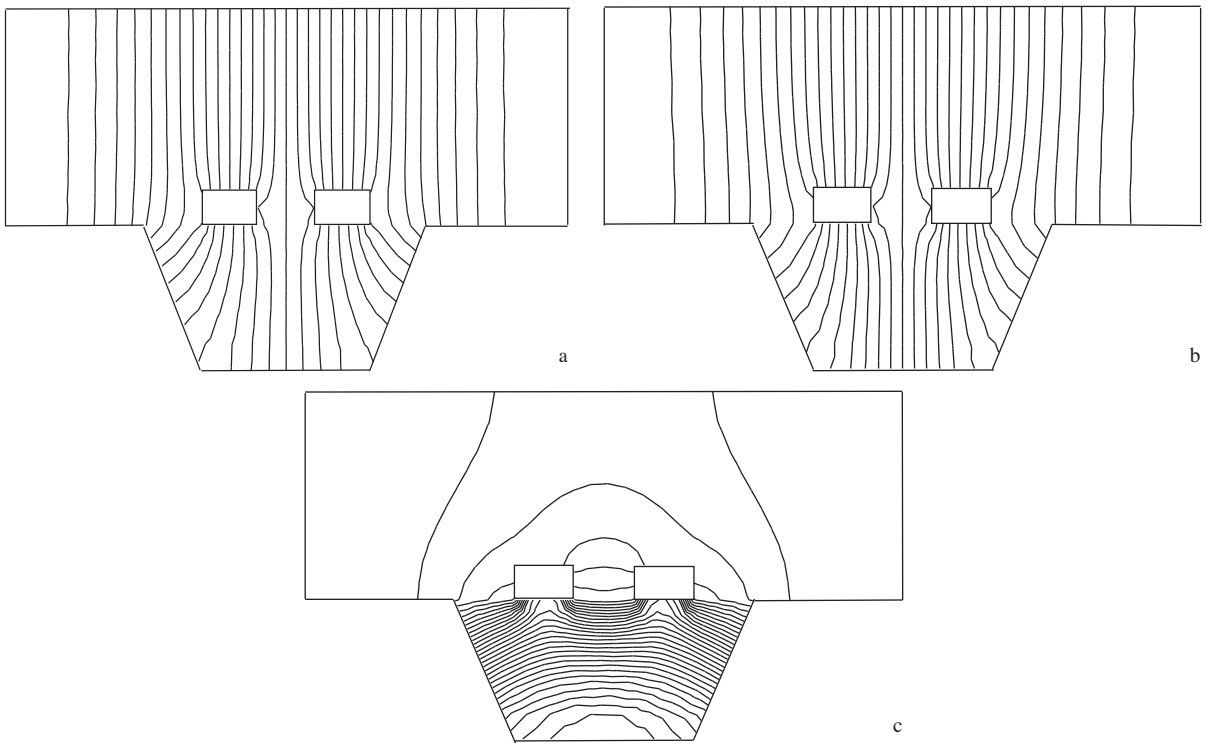

Figure 9. Field patterns of the dominant mode in TML-D for symmetrical metallic signal strips ($c/a = 0.3, c_1/a = c_2/a = c_3/a = 0.1, c_4/a = 0.25, t_1/a = 0.05, t_2/a = 0.05, b_1/a = b_2/a = 0.1$): a)$\varepsilon_r = 2.55$; b)$\varepsilon_r = 5$; c)$\varepsilon_r = 10$.

6 For fixed c/a, c_1/a, c_2/a, c_3/a, b_1/a, b_2/a, t_1/h_1, andt_2/h_1, the cutoff wavelengths decrease as c_4/a increases from 0.05 to 0.3.

7 When the positions of 2 metallic signal strips are symmetric, both the electric field lines of the dominant mode and of the first-higher-order mode are split into 2 symmetrical parts.

8 When the positions of 2 metallic signal strips are asymmetric, the electric field lines of the dominant mode are mainly distributed around the thicker metallic signal strip, while the electric field lines of the first-higher-order mode are mainly concentrated in the dielectric substrate.

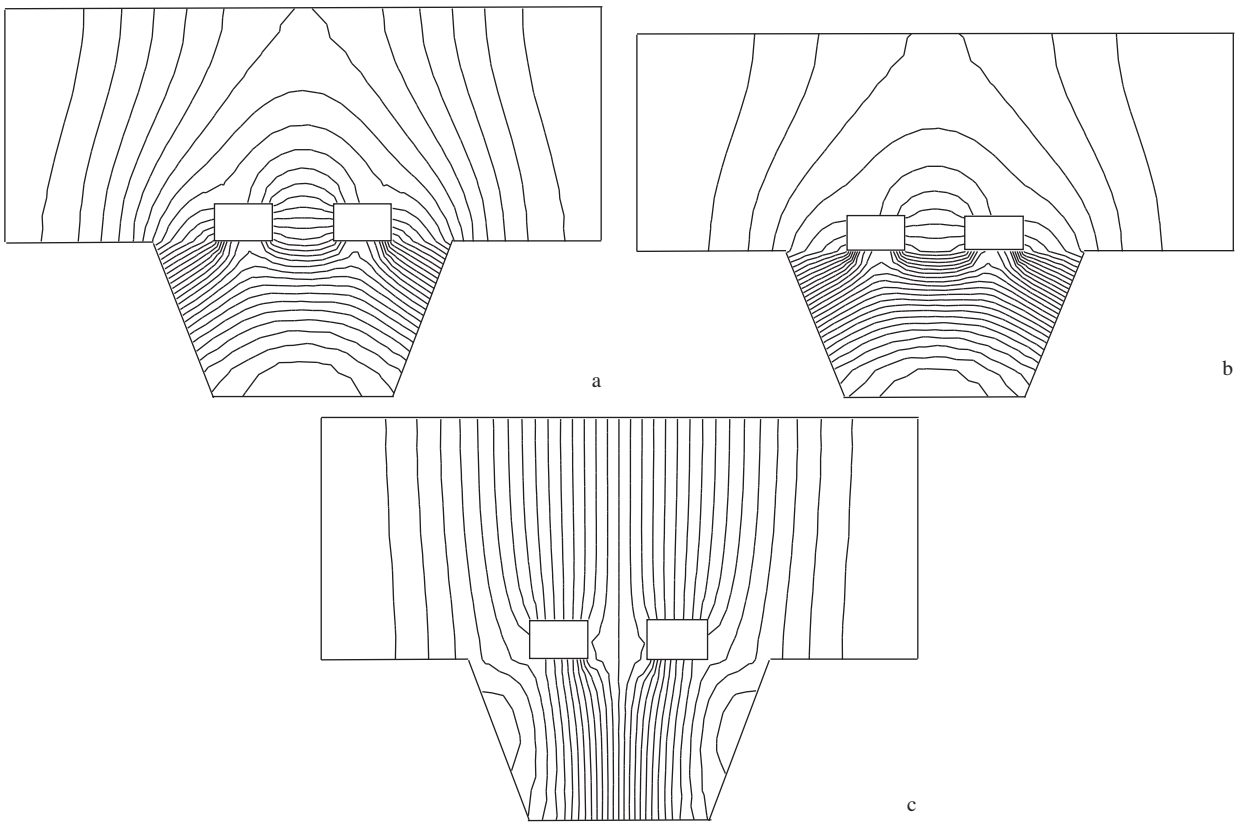

Figure 10. Field patterns of the first-higher-order mode in TML-D for symmetrical metallic signal strips ($c/a = 0.3, c_1/a = c_2/a = c_3/a = 0.1, c_4/a = 0.25, t_1/a = 0.05, t_2/a = 0.05, b_1/a = b_2/a = 0.1$): a)$\varepsilon_r = 2.55$; b)$\varepsilon_r = 5$; c)$\varepsilon_r = 10$.

3.3. The cutoff wavelength of the dominant mode and the field patterns in TML-T

Figures 13-15 show the variations of the normalized cutoff wavelength of the dominant mode in TML-T for different values of t_1/h_1, t_2/h_1, t_3/h_1, b_1/a, b_2/a, b_3/a, c_1/a, c_2/a, c_3/a, and c_5/a. Figures 16-19 show the field patterns of the dominant mode and the first-higher-order mode in TML-T for different ε_r values. From these Figures, we can see:

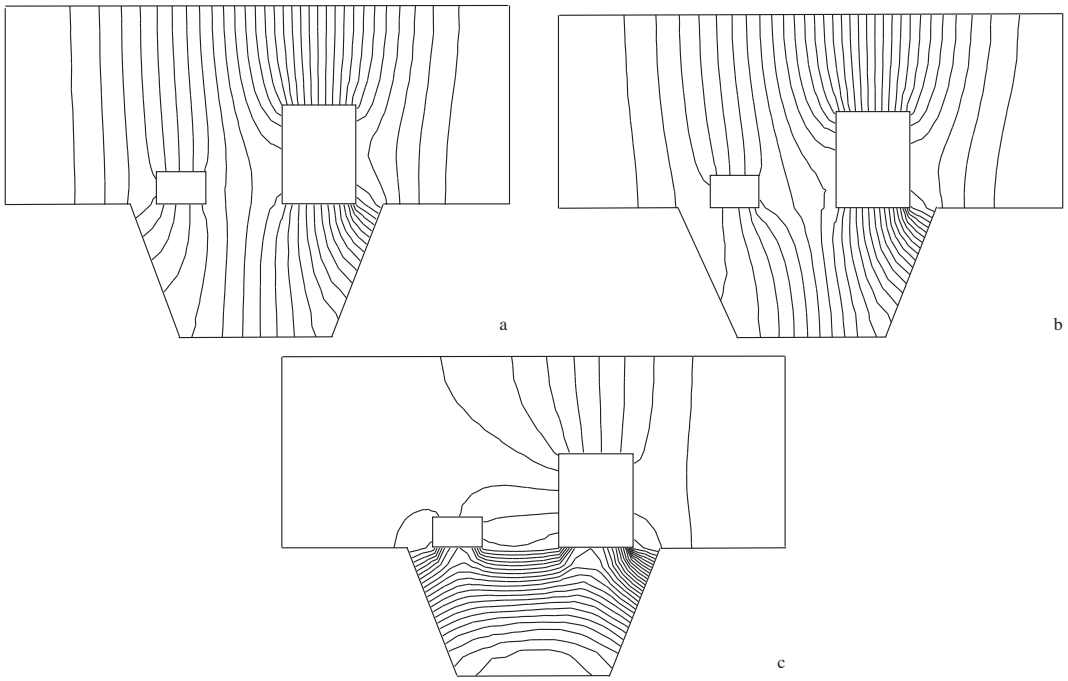

Figure 11. Field patterns of the dominant mode in TML-D for asymmetrical metallic signal strips ($c/a = 0.3, c_1 = 0.05, c_2 = 0.1, c_3 = 0.05, c_4/a = 0.25, t_1/a = 0.05, t_2/a = 0.15, b_1/a = 0.1, b_2/a = 0.15$): a)$\varepsilon_r = 2.55$; b)$\varepsilon_r = 5$; c)$\varepsilon_r = 10$.

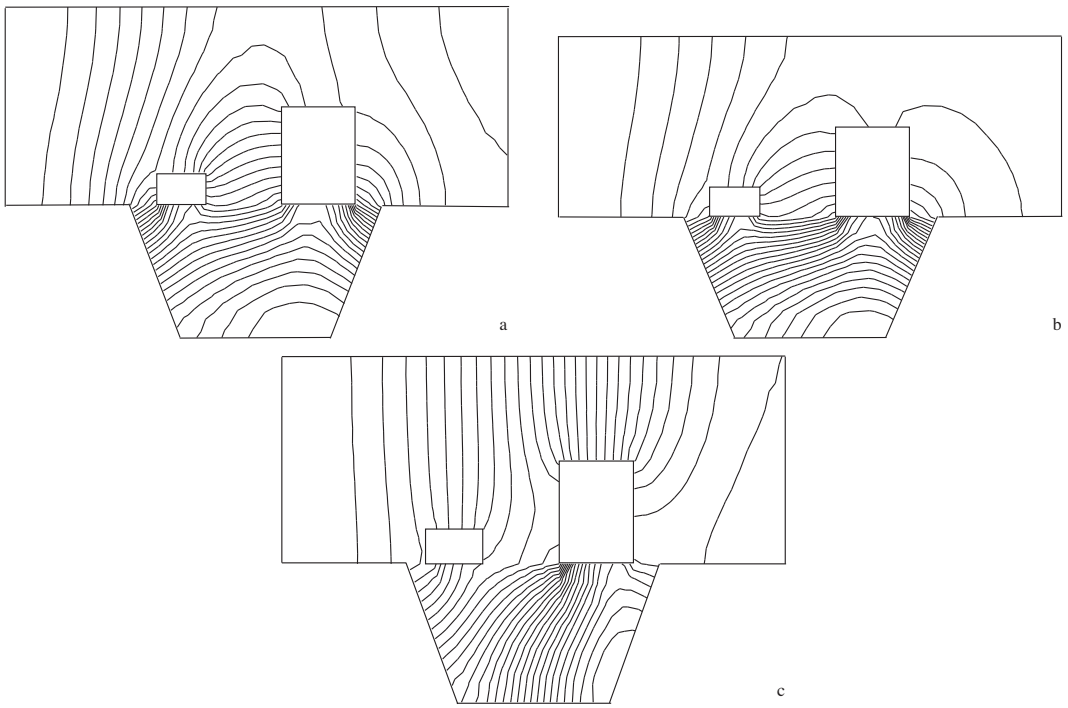

Figure 12. Field patterns of the first-higher-order mode in TML-D for asymmetrical metallic signal strips ($c/a = 0.3, c_1 = 0.05, c_2 = 0.1, c_3 = 0.05, c_4/a = 0.25, t_1/a = 0.05, t_2/a = 0.15, b_1/a = 0.1, b_2/a = 0.15$): a)$\varepsilon_r = 2.55$; b)$\varepsilon_r = 5$; c)$\varepsilon_r = 10$.

1. For fixed c/a, c_1/a, c_2/a, c_3/a, c_4/a, c_5/a, b_1/a, b_2/a, and b_3/a, the values of normalized cutoff wavelengths of the dominant mode increase as t_2/h_1, t_3/h_1, $t_2/h_1 = t_3/h_1$, and $t_1/h_1 = t_2/h_1 = t_3/h_1$ increase from 0.1 to 0.9.

2. For fixed c/a, c_1/a, c_2/a, c_3/a, c_4/a, c_5/a, t_1/h_1, t_2/h_1, t_3/h_1, the cutoff wavelengths first decrease and then increase as b_1/a and $b_1/a = b_3/a$ increase.

3. For fixed c/a, c_1/a, c_2/a, c_3/a, c_4/a, c_5/a, t_1/h_1, t_2/h_1, and t_3/h_1, the cutoff wavelengths increase as b_2/a and $b_1/a = b_2/a = b_3/a$ increase.

4. For fixed b_1/a, b_2/a, b_3/a, t_1/h_1, t_2/h_1, and t_3/h_1, the cutoff wavelengths increase as c_1/a, c_2/a, c_3/a, and c_5/a increase. One point that needs to be emphasized is that when c_1/a and c_2/a increase from 0.45 to 0.5 and c_3/a increases from 0.3 to 0.35, the cutoff wavelengths increase very fast.

5. When the positions of 3 metallic signal strips are symmetric, the field patterns in TML-T are similar to the case of TML-D.

6. When the positions of 3 metallic signal strips are asymmetric, the electric field lines of the dominant mode are mainly distributed around the thickest metallic signal strip, while the electric field lines of the first-higher-order mode are also similar to the case of TML-D.

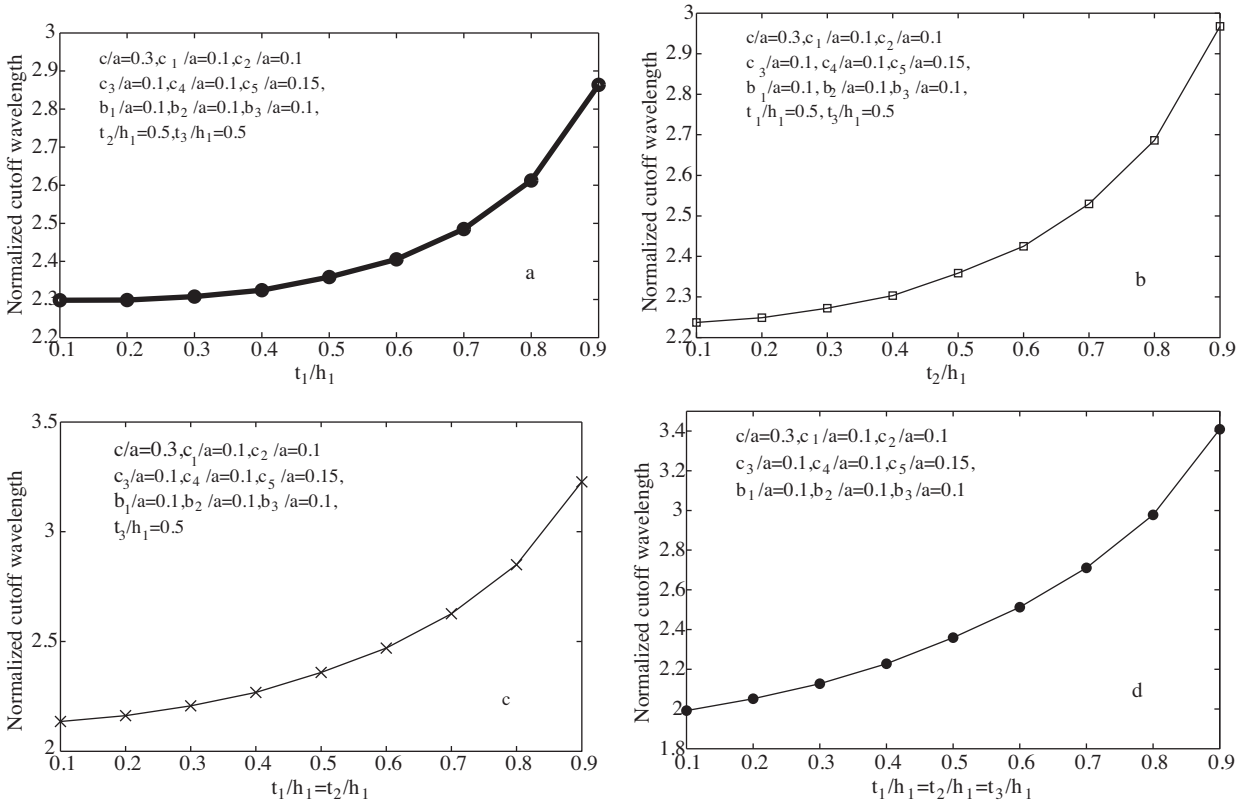

Figure 13. Normalized cutoff wavelength of dominant mode in TML-T: a) versus t_1/h_1; b) versus t_2/h_1; c) versus $t_1/h_1 = t_2/h_1$; d) versus $t_1/h_1 = t_2/h_1 = t_3/h_1$.

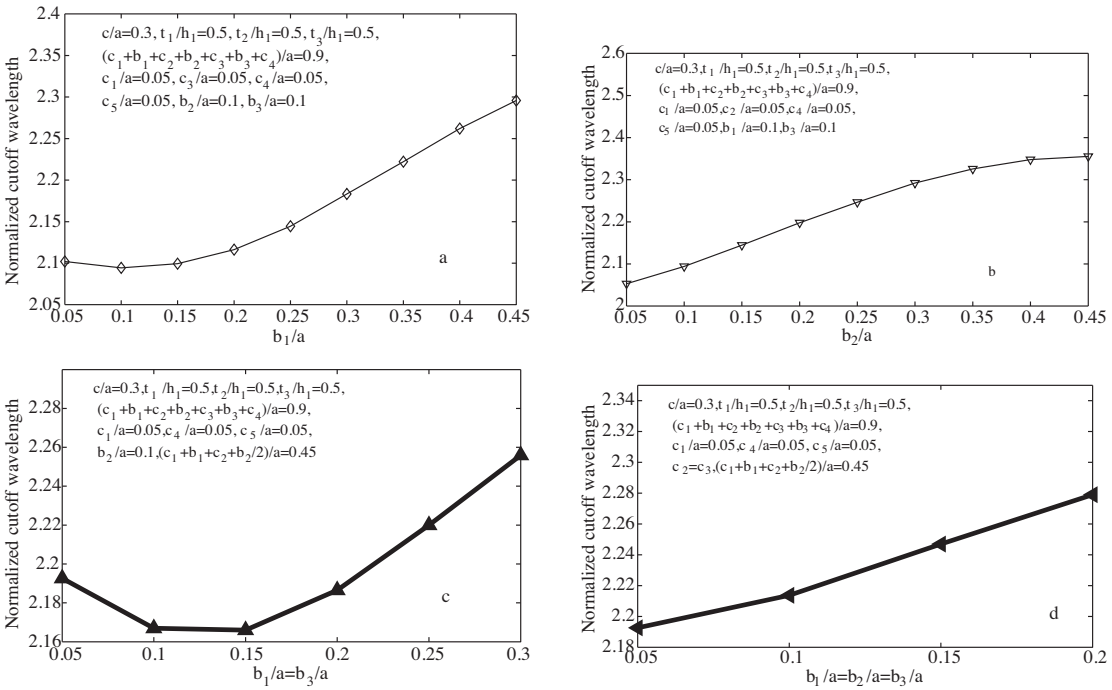

Figure 14. Normalized cutoff wavelength of dominant mode in TML-T: a) versus b_1/a; b) versus b_2/a; c) versus $b_1/a = b_3/a$; d) versus $b_1/a = b_2/a = b_3/a$.

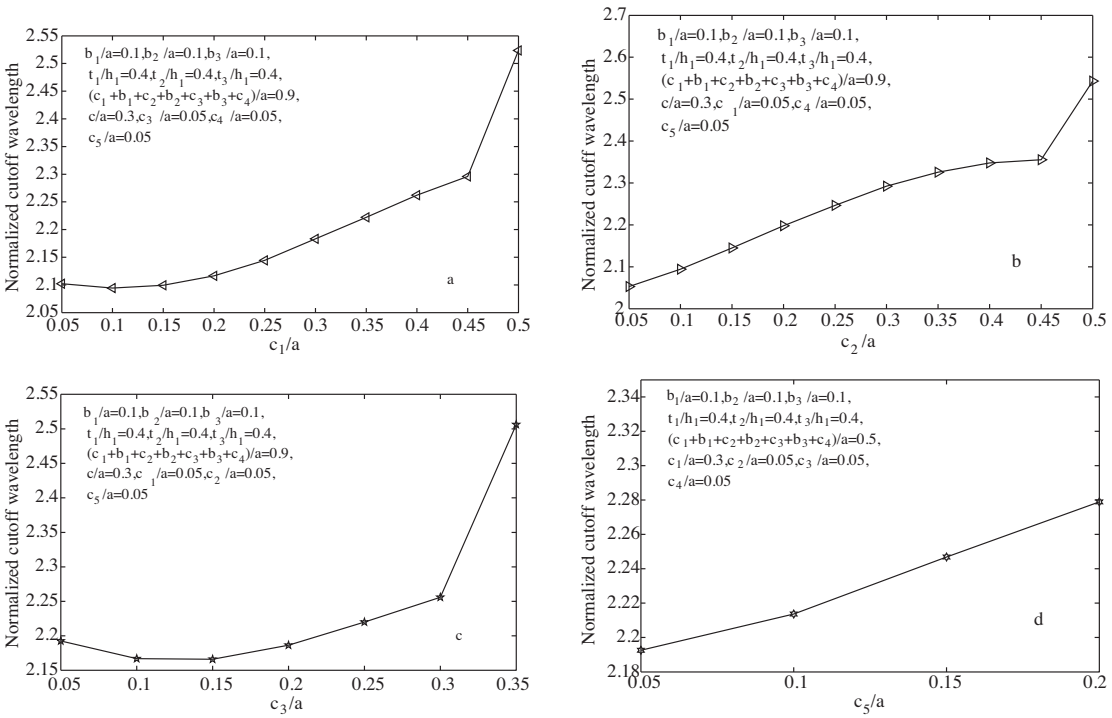

Figure 15. Normalized cutoff wavelength of dominant mode in TML-T: a) versus c_1/a; b) versus c_2/a; c) versus c_3/a; d) versus c_5/a.

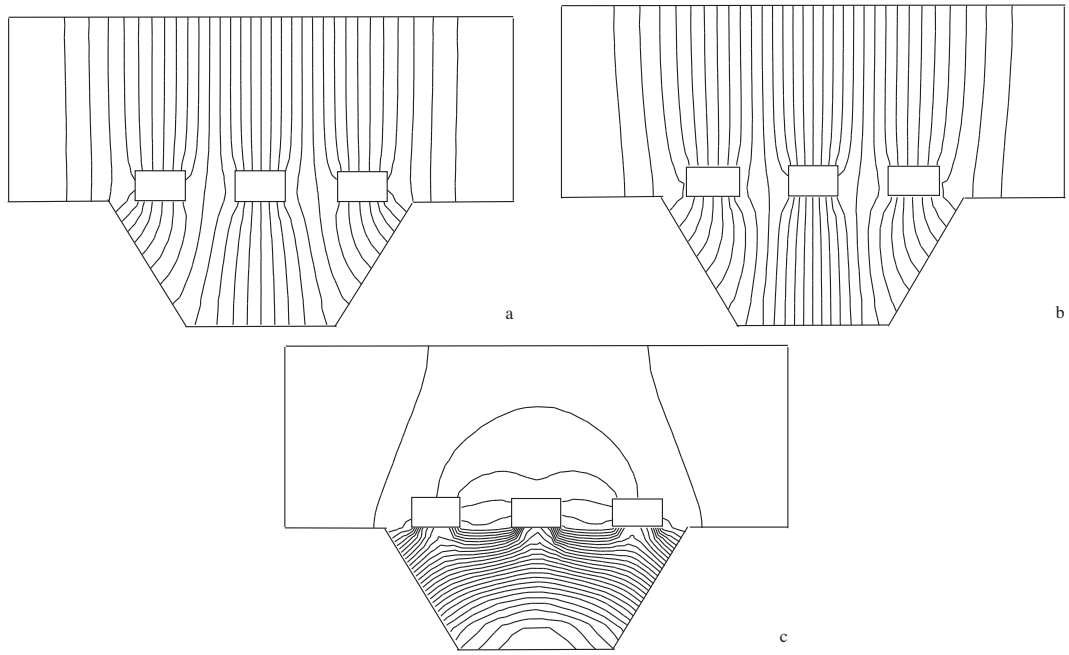

Figure 16. Field patterns of the dominant mode in TML-T for symmetrical metallic signal strips ($c/a = 0.3, c_1/a = c_4/a = 0.05, c_2/a = c_3/a == 0.1, c_5/a = 0.2, (t_1 = t_2 = t_3)/a = 0.05, b_1/a = b_2/a = b_3/a = 0.1$): a)$\varepsilon_r = 2.55$; b)$\varepsilon_r = 5$; c)$\varepsilon_r = 10$.

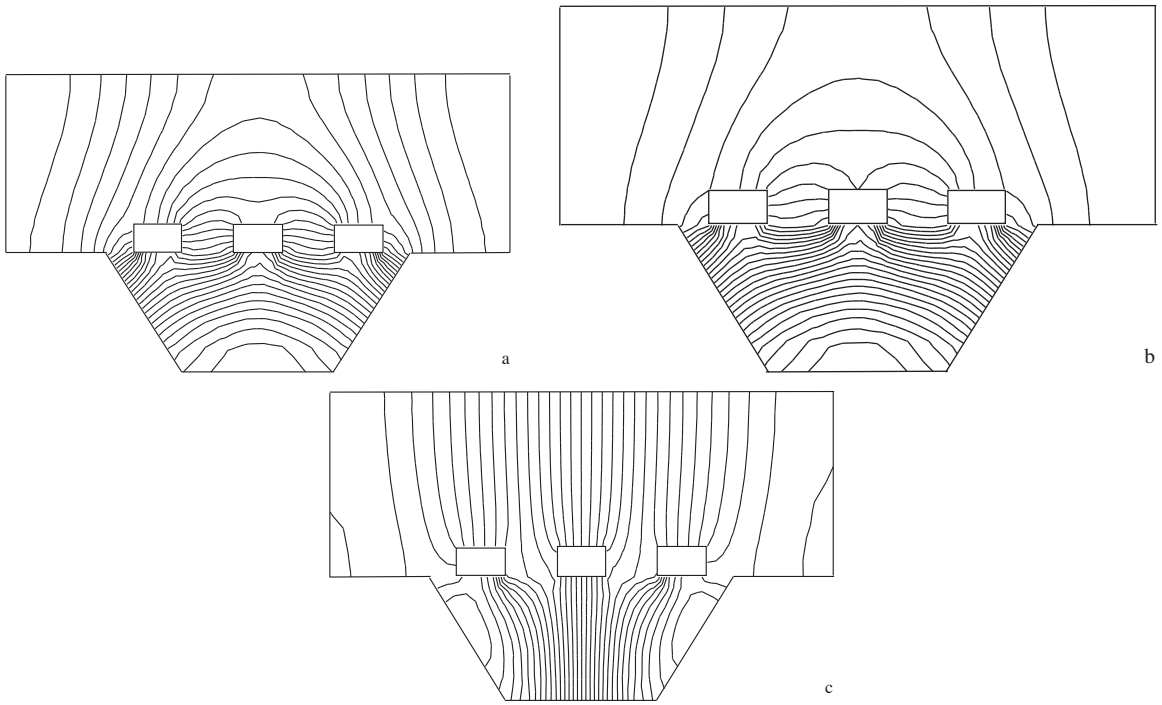

Figure 17. Field patterns of the first-higher-order mode in TML-T for symmetrical metallic signal strips ($c/a = 0.3, c_1/a = c_4/a = 0.05, c_2/a = c_3/a == 0.1, c_5/a = 0.2, (t_1 = t_2 = t_3)/a = 0.05, b_1/a = b_2/a = b_3/a = 0.1$): a)$\varepsilon_r = 2.55$; b)$\varepsilon_r = 5$; c)$\varepsilon_r = 10$.

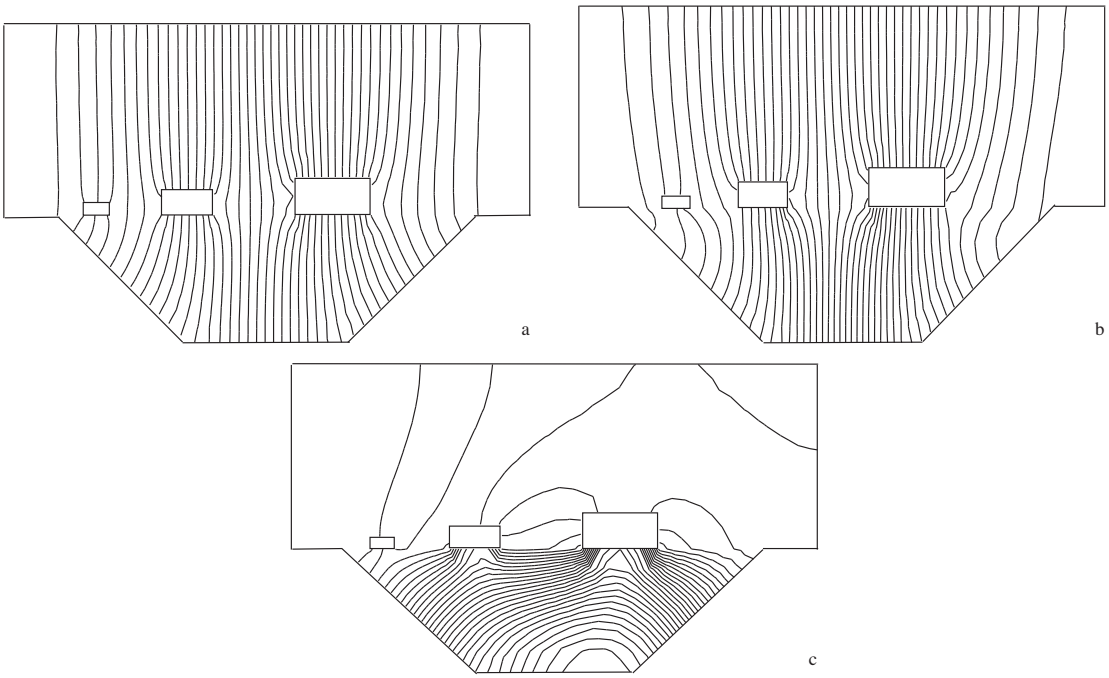

Figure 18. Field patterns of the dominant mode in TML-T for asymmetrical metallic signal strips ($c/a = 0.3, c_1/a = 0.05, c_2/a = 0.1, c_3/a = 0.15, c_4/a = 0.2, c_5/a = 0.1, t_1/a = 0.02, t_2/a = 0.04, t_3/a = 0.06, b_1/a = 0.05, b_2/a = 0.1, b_3/a = 0.15$): a) $\varepsilon_r = 2.55$; b) $\varepsilon_r = 5$; c) $\varepsilon_r = 10$.

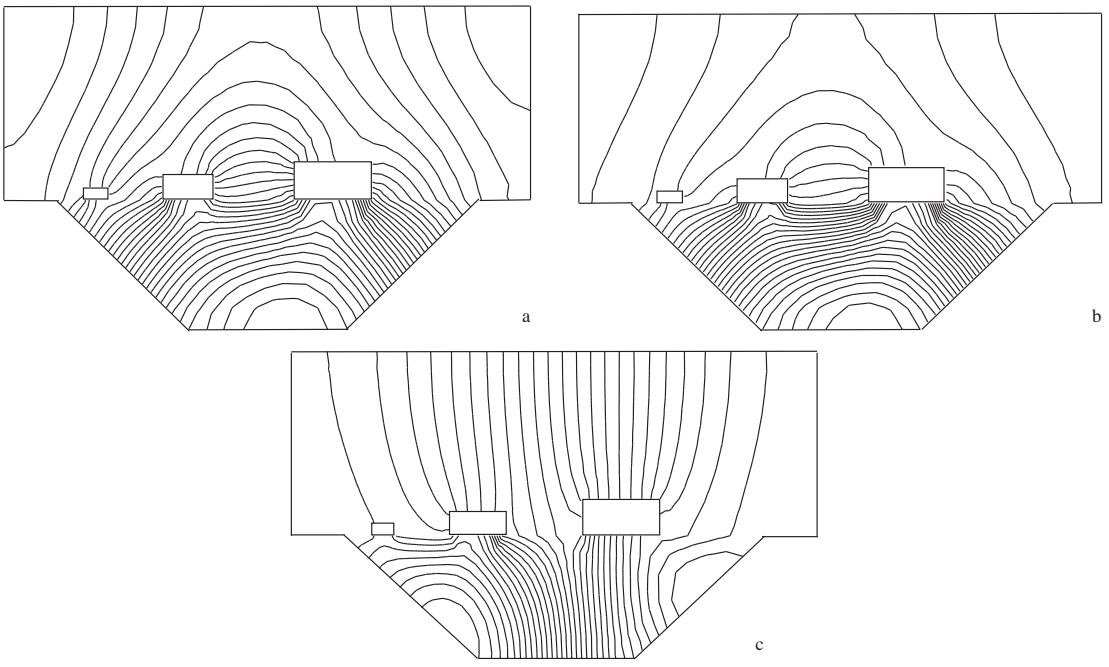

Figure 19. Field patterns of the first-higher-order mode in TML-T for asymmetrical metallic signal strips ($c/a = 0.3, c_1/a = 0.05, c_2/a = 0.1, c_3/a = 0.15, c_4/a = 0.2, c_5/a = 0.1, t_1/a = 0.02, t_2/a = 0.04, t_3/a = 0.06, b_1/a = 0.05, b_2/a = 0.1, b_3/a = 0.15$): a) $\varepsilon_r = 2.55$; b) $\varepsilon_r = 5$; c) $\varepsilon_r = 10$.

7. From the above results, when the value of the dielectric constant of the dielectric substrate increases, the power loss in the dielectric substrate will increase for the dominant mode and decrease for the first-higher-order mode.

4. Conclusion

The cutoff wavelength of the dominant mode and the field patterns in TML-S, TML-D, and TML-T were calculated by the edge-based finite element method. Dependence of cutoff wavelengths and field patterns on different dimensions and the position of the metallic signal strips were presented. The numerical results in this paper have important value in the design of the microshield line in microwave and millimeter-wave integrated circuits.

Acknowledgment

This work was supported by the Educational Commission of Jiangxi Province, China, No. GJJ10169, and by ci-Tech Planning of Gansu Province under Grant No. 0804NKCA073.

References

[1] N.I. Dib, W.P. Harokopus Jr, P.B. Katehi, C.C. Ling, G.M. Rebeiz, "Study of a novel planar transmission line", IEEE MTT-S Digest, Vol. 2, pp. 623-626, 1991.

[2] N.C. Yuan, C.L. Ruan, W.G. Lin, "Analytical analysis of V, elliptical, and circular-shaped microshield transmission lines", IEEE Transactions on Microwave Theory and Techniques, Vol. 42, pp. 855-859, 1994.

[3] K.K.M. Cheng, I.D. Robertson, "Simple and explicit formulas for the design and analysis of asymmetrical V-shaped microshield line", IEEE Transactions on Microwave Theory and Techniques, Vol. 43, pp. 2501-2504, 1995.

[4] Y. Yan, P. Pramanick, "Finite element analysis of generalized V- and W-shaped edge and broadside-edge-coupled shield microstrip lines on anisotropic medium", IEEE Transactions on Microwave Theory and Techniques, Vol. 49, pp. 1649-1657, 2001.

[5] J. Kiang, "Characteristic impedance of microshield lines with arbitrary shield cross section", IEEE Transactions on Microwave Theory and Techniques, Vol. 46, pp. 1328-1331, 1998.

[6] M. Lu, P.J. Leonard, "Design of trapezoidal-ridge waveguide by finite element method", IEE Proceedings Microwaves, Antennas and Propagation, Vol. 151, pp. 205-211, 2004.

[7] M. Lu, P.J. Leonard, "Dependence of ridge position on the cutoff wavelengths of the dominant mode in single ridge waveguides", Microwave and Optical Technology Letters, Vol. 34, pp. 374-377, 2002.

[8] M. Lu, P.J. Leonard, "On the field patterns of the dominant mode in unilateral finline by finite-element method", Microwave and Optical Technology Letters, Vol. 38, pp. 193-195, 2003.

[9] M. Lu, P.J. Leonard, "Edge-based finite element analysis of the field patterns in V-shaped microshield line", Microwave and Optical Technology Letters, Vol. 41, pp. 43-47, 2004.

[10] H. Sun, M. Lu, "Research on transmission characteristics of upswept-ridge waveguide by the FEM", ICMMT International Conference on Microwave and Millimeter Wave Technology, Vol. 2, pp. 512-514, 2008.

[11] J.M. Jin, The Finite Element Method in Electromagnetics, 2nd ed., New York, Wiley, 2002.

[12] J.F. Lee, D.K. Sun, Z.J. Cendes, "Full-wave analysis of dielectric waveguides using tangential vector finite elements", IEEE Transactions on Microwave Theory and Techniques, Vol. 39, pp. 1262-1271, 1991.

[13] S.F. Shu, P.M. Goggans, A.A. Kishk, "Computation of cutoff wave numbers for partially filled waveguides of arbitrary cross section using surface-integral formulations and the method of moments", IEEE Transactions on Microwave Theory and Techniques, Vol. 41, pp. 1111-1118, 1993.